Available online at www.sciencedirect.com

SciVerse ScienceDirect

Ceramics International 39 (2013) 2933–2941

CERAMICS INTERNATIONAL

www.elsevier.com/locate/ceramint

Controllable synthesis of metastable tetragonal zirconia nanocrystals using citric acid assisted sol–gel method

Fatemeh Davar[a,b,*], Asadollah Hassankhani[b], Mohammad Reza Loghman-Estarki[c,*]

[a]Faculty of chemistry, Razi University, Kermanshah, Iran

[b]Department of Materials Science, International Center for Science, High Technology & Environmental Sciences, P.O.Box: 98-76315-117, Kerman, Iran

[c]Department of Materials Engineering, Isfahan University of Technology, Isfahan, Iran

Received 27 July 2012; received in revised form 18 September 2012; accepted 19 September 2012
Available online 17 October 2012

Abstract

Metastable tetragonal ZrO_2 nanoparticles and nanosheets were synthesized with citric acid assisted sol–gel method. In this approach, zirconium acetylacetonato, $Zr(acac)_2$, citric acid (CA) and ethylene glycol (EG) were used as the source of Zr^{4+}, the chelating, and solvent agent, respectively. The effects of heat treatment on zirconia phase evolution were investigated. We demonstrate that pure tetragonal nanocrystalline zirconia can be obtained with CA: EG mole ratio = 5:1 and calcination temperature 490 °C. The microstructure of the products was characterized by X-ray diffractometry (XRD), scanning electron microscopy (SEM), transmission electron microscopy (TEM), selected area electron diffraction (SAED) and Raman scattering. Finally, Photoluminescence (PL) of nanosheets and nanoparticles were also investigated.

Keywords: D. ZrO_2; Ceramic; Sol-gel method; Photoluminescence

1. Introduction

At atmospheric pressure, pure zirconia has three solid polymorphs which exhibit monoclinic structure [space group $P2_1/c$] (m-phase), that is, thermodynamically stable at the temperatures below 1172 °C, tetragonal structure [space group $P4_2/nmc$] (t-phase), stable at the temperature range of 1172–2347 °C, and cubic structure [space group $Fm3m$] (c-phase), stable above 2347 °C [1–3]. The applications of zirconia strongly depend on both crystal structure and phase transformations [3–5]. Cubic phase of zirconia is a good candidate for solid oxide fuel cells (SOFCs), oxygen sensors, electrochemical capacitor electrodes and ferrules due to its ionic, electrical [3,4,6] and optical [7] properties. Tetragonal zirconia can be used as an effective catalyst due to unique amphoteric characteristics and redox properties [7,8]. The transformable tetragonal zirconia, such as yttria stabilized zirconia (YSZ) (called t-phase) used as engineering ceramic material since it shows high values of strength and hardness. This hardening mechanism is due to the transformation of the tetragonal phase into the monoclinic phase which implies a volume change associated with pseudo-plasticity [5,9]. The 'non-transformable' metastable tetragonal YSZ phase (called t′) [5] is remarkably resistant and does not undergo the transformation to the monoclinic phase under stresses. The t′ phase is widely used for thermal barrier applications due to the formation of a tweed microstructure which tends to increase the thermo-mechanical performances [10]. This microstructure corresponds to a three-dimensional pseudo-periodic lattice of high Y_2O_3 cubic particles within all of the t′ grains [5].

There are five techniques for obtaining metastable tetragonal phase of zirconia at room temperature: (1) stabilization with doping metal oxide, such as Y_2O_3 doped zirconia (YSZ) [10–15] (2) Using high rate deposition techniques, such as EBPVD, plasma spray method: In these techniques, the t′ phase is obtained via a displacive transformation by quenching liquid or cubic phase from high temperature

*Corresponding authors at: Isfahan University of Technology, Faculty of chemistry, Isfahan, Iran. Tel.: +98 913 3635478; fax: +98 3113886.

E-mail addresses: f.davar@gmail.com (F. Davar), mr.loghman@ma.iut.ac.ir (M.R. Loghman-Estarki).

0272-8842/$ - see front matter © 2012 Elsevier Ltd and Techna Group S.r.l. All rights reserved.
http://dx.doi.org/10.1016/j.ceramint.2012.09.067

[16,17](3) crystallization from amorphous phase [18,19] (4) particle or crystallite size reduction of zirconia to 8–29 nm and below 5 nm, respectively [5,20–23]; and (5) thermal decomposition of zirconium salts, alkoxides and hydroxide or by ball milling of monoclinic zirconia (m-ZrO_2). There are some evidences that metastable t-ZrO_2 can also be produced by ball milling of zirconium decomposition products of three different zirconium salts [7].

The high-temperature cubic and tetragonal phases can be stabilized at room temperature by incorporating dopants in the lattice, e.g., CaO, MgO, Y_2O_3 and CeO_2 [10–15]. However, it is difficult to stabilize these high-temperature phases at room temperature without any doping. Particle size reduction is known to stabilize the high-temperature modifications at room temperature. It has been reported in the literature that in the case of nanopowders above the critical size of 20–30 nm, the material reverts to monoclinic (m-) ZrO_2 [20–25]. It was concluded that the formation of t-ZrO_2 is dependent on the nature of starting salt, the type of synthetic method and the crystallite size of zirconia [9]. As it was said before, the stable phase of zirconia at room temperature (RT) is monoclinic. So, it is very important to control zirconia crystallite size to obtain tetragonal structure at RT. One of the effective methods is citric acid and ethylene glycol-based process, which is established for the preparation of fine ceramic oxide powders. In this technique, a uniform particle size powder is produced by means of a homogeneous distribution of metal ions in the polymeric gel. The polymeric (polyester) gel produced by the reaction of citric acid and ethylene glycol during heat treatment. Meanwhile, other elements such as C and H are easily removed during calcination. Therefore, the purity of the final powder will not get affected when citric acid and ethylene glycol are being used as chelating agents and template materials [24].

The main goal of the present research is the synthesis of nano size tetragonal zirconia powder via introducing zirconium acetylacetonato, $Zr(acac)_2$, as a new starting salt for producing homogenous gel. Also, the effects of particle size on the zirconia phase evolution are investigated. Finally, the optical properties of ZrO_2 nanosheets and nanoparticles are investigated.

2. Experimental

2.1. Materials

All of the materials purchase from Merck Company (Germany) and were used as received without further purification.

2.2. Characterization equipment

XRD patterns (X'Pert Pro, Philips, Holland) were recorded by a Rigaku D-max C III, X-ray diffractometer using Ni-filtered Cu K_α radiation ($\lambda = 1.5406$ Å), generator setting 40 kV and 30 mA and step size 0.05. Field emission scanning electron microscopy (FESEM) images were obtained on S-4160 (Hitachi Ltd., Japan). Transmission electron microscopy (TEM) micrographs were obtained on a Philips EM208 transmission electron microscope with an accelerating voltage of 100 kV. Samples for TEM were prepared by diluting the product with ethanol and placing a 6 μL drop onto a 200 mesh copper grid covered by a continuous amorphous carbon film. Analysis of particle size was done with the Scion image Beta 4.02 software for image processing. Crystallite sizes (D_c) were calculated from the line broadening of the X-ray diffraction peaks using the Debey–Scherrer Eq. (1) [3,20],

$$D_c = k\lambda/\beta\cos\theta \quad (1)$$

where β is the breadth of the observed diffraction line at its half-intensity maximum, k is the so-called shape factor, which usually takes a value of about 0.9, and λ is the wavelength of X-ray source used in XRD.

2.3. Synthesis of nanocrystalline zirconia

In a typical experiment, 3 g $Zr(acac)_2$ and citric acid mono hydrate ($C_6H_8O_7$. H_2O) were dissolved in deionized water, and appropriated amounts of ethylene glycol (EG) were then added (EG:CA mole ratios = 1:1, 5:1, 20:1) to form a sol at 50 °C for 1 h (The pH value of precursor was ~2). A white solution was obtained and further heated at 80 °C for 1 h to remove excess water. During continued heating at 140–150 °C for 1 h, the solution became more and more viscous and finally became a xerogel. To complete drying, xerogel was placed at 250 °C for 1 h. The result powder is a precursor. In the furnace, the precursor was calcined at 490–650 °C for 2 h, in an alumina boat, and then was cooled to reach room temperature. To investigate pH effect on the morphology and phase structure, in parallel reactions series, the pH value was changed from 2 (acidic medium) to 12 (alkali medium), by adding adequate liquor ammonia (for changing pH of precursor, 120 ml concentrated ammonia was added, so the final pH of solution was adjusted at 12.) and other parameters such as EG:CA ratio and calcination temperature were kept constant.

3. Results and discussion

3.1. The effect of the calcinations temperatures

It is well known that calcination can result in the growth of zirconia crystallite. In order to investigate the effect of temperature on the crystallization process of zirconia, XRD results of zirconia, calcined at 650, 540 and 490 °C for 2 h, respectively, were compared. Fig. 1a shows XRD of as-prepared products at 650 °C. This figure indicates that a mixture of monoclinic (m) and tetragonal (t) phase of zirconia was obtained. When calcinations temperature was reduced to 540 °C (Fig. 1b) the amount of m-phase was considerably reduced. Upon reducing temperature to 490 °C (Fig. 1c), no m-phase was obtained. The distinguishing characteristic peaks for t-phase occur at $2\theta = 30.2°$, 34.9°, 50.6° and 60.08° for the (1 0 1), (0 0 2),

(2 0 0) and (2 1 1) reflections [5,9,16,17]. So, all XRD pattern of as-prepared sample, calcined at 490 °C, was indexed as a t-phase of zirconia. This is very close to the values in the literature (JSPDS No. 01-080-2155, $a=b=0.36067$ and $c=0.5129$ nm, space group P_{42}/nmc) and no impurity such as C, Zr(acac)$_2$, etc., was found in X-ray diffraction pattern.

The crystallite sizes (Table 1) of the as-prepared products, calculated with Scherer formula, were continuously reduced by decreasing the reaction temperature from 650 to 490 °C. As can be seen in Table 1, the average crystallite size of all products was between 13 and 25 nm, but XRD results showed that the phase of one of the products was pure tetragonal. These results showed that achieving pure t-phase was highly sensitive to crystallite size [5,20,23].

The tetragonal structure can be obtained from the cubic structure wherein one of the axes of the cubic fluorite structure is elongated and correspondingly oxygen anions are displaced from their ideal positions along the direction of elongation. This is observed as splitting of some of the XRD peaks. However, in the case of nanopowders, due to the inherently broad nature of the peaks, splitting is not very evident. In other hand, the cubic and tetragonal structures ($a=0.5124$ nm for cubic, and $a=0.5094$ and $c=0.5177$ nm for tetragonal structures) are very similar [27]. So, the assignment of cubic and tetragonal structures, based solely on the X-ray diffraction analysis, can be difficult. The literature [27–29] reported that the tetragonal structure can be distinguished from the cubic structure in the presence of characteristic splitting of the tetragonal phase, such as (0 0 2)/(2 0 0), (1 1 3)/(3 1 1) and (0 0 4)/(4 0 0) at 2θ 35.1°, 60.02° and 73.4°, respectively, whereas the cubic phase exhibits only single peaks at all of these positions. In Fig. 1c, no splitting was observed at the aforementioned 2theta. So, it was concluded that the cubic phase of ZrO_2 was obtained, but we have found that particle size broadening of XRD profiles can lead potentially to incorrect structural assignments. It is therefore concluded that a more complete analysis including Raman spectroscopy in addition to XRD, should be undertaken before positively assigning the crystal structures of materials with very small crystallite size [28,29].

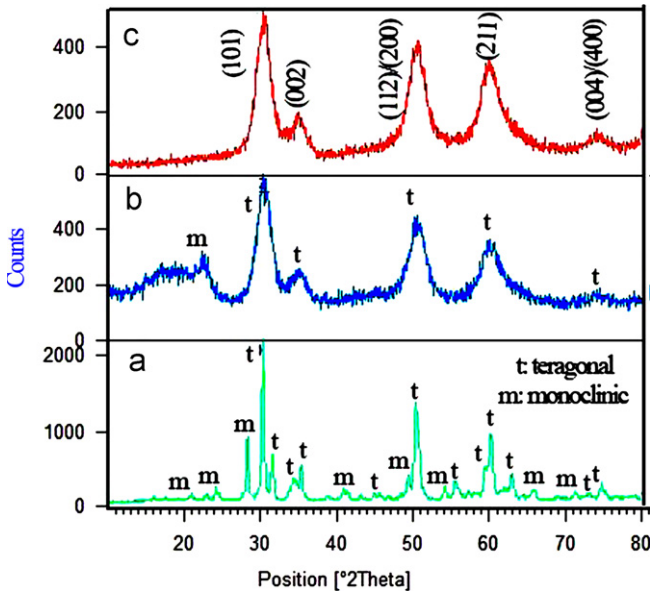

Fig. 1. XRD of the as-prepared samples at different temperatures (a) 650 °C, (b) 540 °C (c) 490 °C.

The cubic to tetragonal phase transition in zirconia occurs by an elongation of the crystallographic c axis and a concomitant displacement of the oxygen atoms from the ideal anion sites in the fluorite structure. Raman spectroscopy is sensitive to the polarizability of the oxygen ions and therefore, it can be used to determine the symmetry of a crystal system. Raman spectroscopy is a nondestructive experimental technique for probing the vibrational and structural properties of materials. It is also recognized as a powerful tool for identifying different polymorphs of metal oxides [2,27]. According to group theory, monoclinic (m-ZrO_2), tetragonal (t-ZrO_2) and cubic phase of zirconia (c-ZrO_2) are expected to have 18 (9Ag+9Bg), 6 ($1A_{1g}+2B_{1g}+3E_g$) and one T_{2g} Raman active modes [27]. Fig. 2 is the Raman spectra as-obtained products at 650 °C (Fig. 2a) and 490 °C (Fig. 2b), using the laser with 532 nm. According to Fig. 2a, peaks in 153 (B_{1g} mode of t-phase) 356 (m-phase), 453 (t- and m-phase) and 629 cm^{-1} (m- and t-phase) shows mixture of monoclinic and tetragonal phase exists in the sample calcined at 650 °C. Upon reducing calcinations temperature to 490 °C, the characteristic of m-phase do not exist in the sample and the peaks located at 153, 330, 410 and 640 cm^{-1} confirms t-phase of zirconia successfully obtained. It should also noted that six Raman frequencies of t-ZrO_2 at different literature are in the range of (i)145 (E_g mode)-155 (B_{1g}), (ii) 240 (E_g)–266 (A_{1g}), (iii) 290 (B_{1g})–326 (E_{1g}) (iv) 410 (E_{1g})–466 (E_g) (v) 550 (A_{1g})–616 (B_{1g}) (vi) 615 (E_g)–645 (E_g) [27–34]. The frequencies of four types of zirconia phase are summarized in Table 2. According to Fig. 2b, the peaks at 153 (B_{1g} mode), 330 (E_{1g} mode), 410 cm^{-1} (E_{1g} mode) and 640 cm^{-1} (E_g mode) are

Table 1
The crystallite size of as-prepared product at different temperatures.

Temp. (°C)	FWHM of (1 0 1)	FWHM of (2 0 0)	FWHM of (2 1 1)	Grain size (nm)	Phase (XRD)
650	0.2952	0.2952	0.3936	27.5	T+m
540	0.4920	0.3389	1.2	16.7	T+m
490	0.4920	0.7200	0.8288	13.4	T

corresponded to t-phase of zirconia. The absence of other two main peaks (290 and 550 cm^{-1}) of t-zirconia probably was related to more symmetry of our obtained t-phase than other similar works or peaks overlapping. Research show the strong peak at 530–640 (with 550 maximum) and 460 cm^{-1} are related to cubic phase of zirconia [25]. The absence of this peak in the sample calcined at 490 °C show c-phase did not exist in this sample.

In order to investigate the effect of heat treatment on the morphology and particle size of nanocrystalline zirconia, SEM images of zirconia, calcined at 650, 540 and 490 °C for 2 h, respectively, were compared. Fig. 3a shows SEM image of as-prepared products at 650 °C. This figure indicates that agglomerated particles with average size being between 40 and 50 nm were obtained. By reducing calcinations temperatures to 540 and 490 °C, the particle size of as-prepared samples was reduced to 40–45 nm (Fig. 3b) and 15–20 nm (Fig. 3c), respectively.

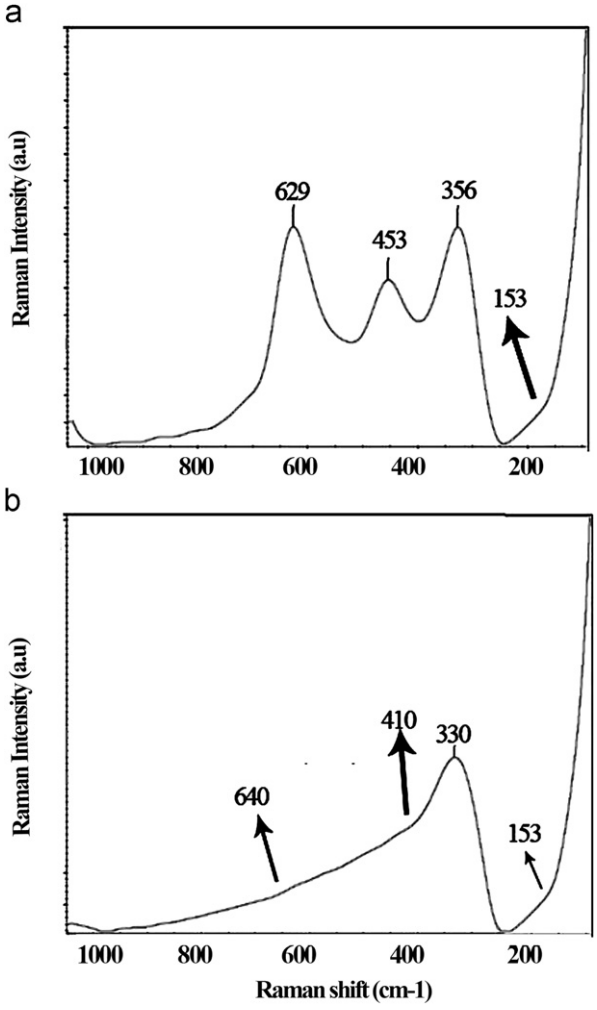

Fig. 2. (a) Raman spectra as-obtained products at 650 °C and (b) 490 °C.

The presence of tetragonal phase in as-prepared ZrO_2 and the powder formed at low temperature is attributed to the fact that the specific surface free enthalpy of tetragonal ($\gamma = 0.77$ J/m^2) is smaller than that of monoclinic ($\gamma = 1.13$ J/m^2). The large surface area of as-synthesized nanopowders becomes a thermodynamic barrier for t-ZrO_2 to m-ZrO_2 phase transformation. Consequently, tetragonal phase is remained. Liang et al. [34] explained the formation of tetragonal phase at low temperature is attributed to that the structure of zirconia precursor is regarded as hydrous zirconia ($ZrO_2.nH_2O$) and the schematic structure unit has 16 zirconium atoms, 20 non-bridging hydroxogroups, 22 bridging oxide bond and 20 coordinated water. Based on this model, the following equations are obtained by decreasing the temperature to 490 °C [35]:

$$[Zr_{16}O_{22}(OH)_{20}(H_2O)_{20}] \times xH_2O \overset{\text{Naturally dried}}{\Rightarrow} [Zr_{16}O_{22}(OH)_{20}(H_2O)_{20}] + xH_2O \quad (2)$$

$$[Zr_{16}O_{22}(OH)_{20}(H_2O)_{20}] \times xH_2O \overset{\text{Naturally dried}}{\Rightarrow} [Zr_{16}O_{22}(OH)_{20}(H_2O)_{20}] + xH_2O$$
$$[Zr_{16}O_{22}(OH)_{20}(H_2O)_{20}] \overset{\text{Heat}}{\Rightarrow} 16ZrO_2 + 30H_2O \quad (3)$$

when the citric acid based gel is heated up to about 490 °C, the metastable tetragonal zirconia is observed compared to its stable temperature around 1100–2370 °C. The amorphous to tetragonal phase transformation is attributed to the loss of water from the amorphous hydrous zirconia resulting from the release of water of hydration and the production of water via oblation [27].

3.2. Effect of EG:CA mole ratio

3.2.1. SEM analysis

The effects of the mole ratio of ethylene glycol (EG) to citric acid (CA) in the starting solution on the morphology and particle size of the samples are shown in Fig. 4. Fig. 4a illustrates the morphology of the powder obtained from the EG:CA mole ratio 1:1. This sample is consisted of relatively compact large particles that showed flat faces and angular edges. High magnification of the faces in Fig. 4b revealed that the as-formed products consisted of nanometer grains (~60 nm diameter). When EG:CA mole

Table 2
Raman shift of different modifications of zirconia.

Zirconia phase	Raman shift (cm^{-1})	Mode	Reff.
Amorphous	550–600 (broad)	—	[23]
Monoclinic	98–102, 180–189, 220, 178, 189, 225, 300, 335, 380, 475, 535, 555, 615, 635	$9Ag+9Bg$	[28]
Tetragonal	131–155, 240–266, 290–330, 410–475, 550–615, 616–645	$1A_{1g}+2B_{1g}+3E_g$	[27]
Cubic	250–280, 464–490, 530–640 (maximum at 550)	T_{2g}	[27]

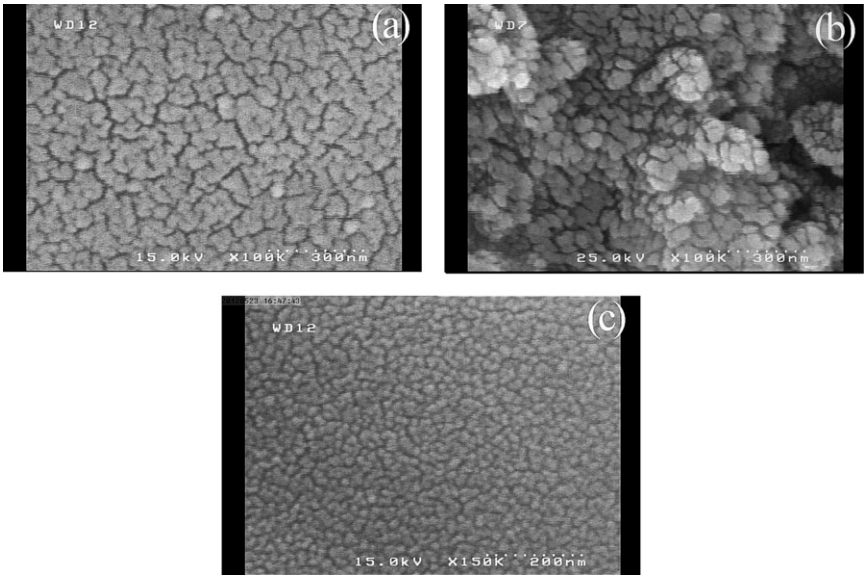

Fig. 3. SEM images of Zirconia nanocrystals at different calcinations temperatures (a) 650 °C (b) 540 °C (d) 490 °C.

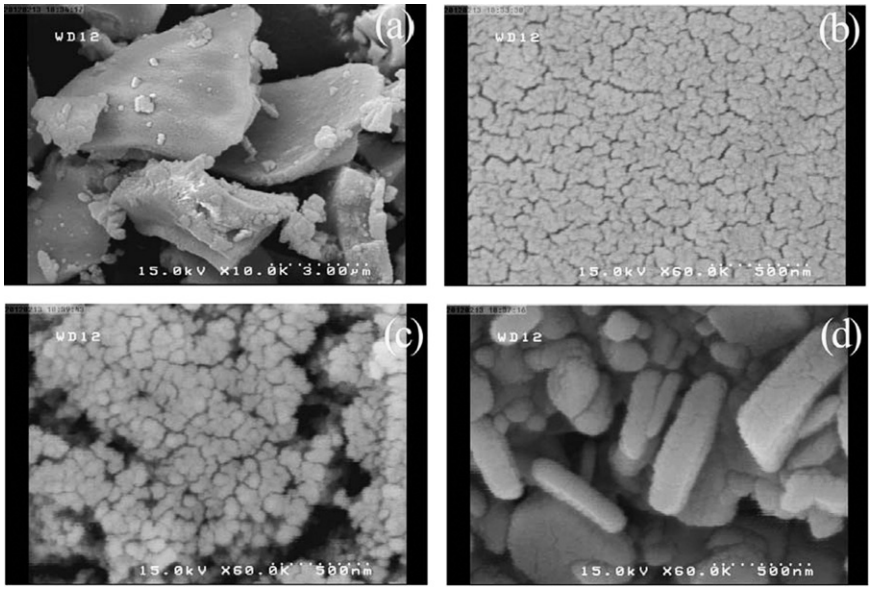

Fig. 4. SEM images of zirconia nanocrystals with various EG:CA mole ratios calcined at 490 °C (a and b) 1:1 (c) 5:1 (d) 20:1.

ratio was 5:1, the sample was consisted of particles with average diameter ~50 nm. The scanning electron microscopy images showed a clear change in the morphology as the EG:CA mole ratio was increased from 5:1 (Fig. 4c) to 20:1 (Fig. 4d). According to Fig. 4d, nanosheets with a width of ~40 nm and a length up to 1 μm were obtained. To the best of our knowledge, this is the first report on the synthesis of zirconia nanosheets via citric acid-based gel. These results show how EG:CA mole ratio could change the shape and particle size of as-prepared zirconia samples.

3.3. The effect of pH

The effects of pH in the starting solution on the morphology and particle size of samples are shown in Fig. 5. The morphologies of the products were changed obviously by altering pH medium from one of acidic to alkali one. When calcination temperature was 490 °C, the particle morphology was changed from semispherical particles with 15–20 nm in diameters, (observed at low pH ~2, Fig. 5a), to nanoshees with width of 30–40 nm and length up to 500 nm (observed at pH 12, Fig. 5b). Upon increasing calcination temperature from 490 to 650 °C, the sample prepared at acidic alkali medium consisted of desegregated fine particulates, with ~50 nm diameters, (Fig. 5c). A close look at Fig. 5b was also showed that nanosheets are composed of numerous nanoparticles. It seems that with increasing calcinations temperature from 490 to 650 °C, nanosheets were broken to nanoparticles. For the alkali precursors (pH=12) (Fig. 6), the sample

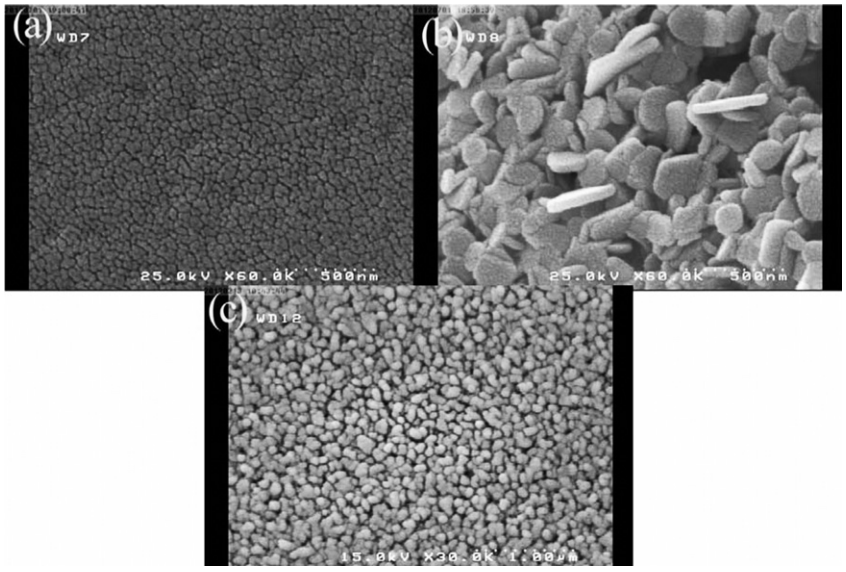

Fig. 5. SEM images of zirconia nanocrystals with EG:CA mole ratios 5:1 calcined at 490 °C at different pH (a) ~2 (b) 12 and calcined at 650 °C with (c) acidic medium (d) alkali medium.

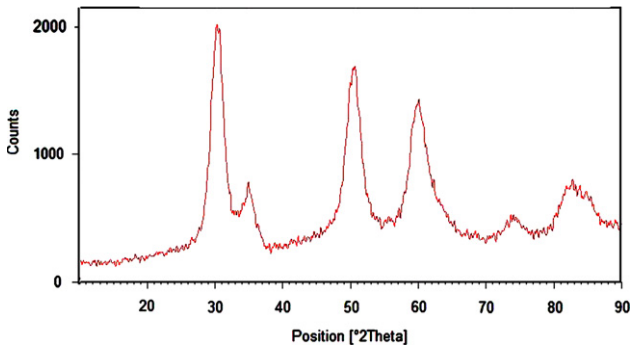

Fig. 6. XRD pattern of zirconia nanocrystals with EG:CA mole ratios 5:1 calcined at 490 °C at alkali pH.

calcined at 490 °C for 2 h, is also composed of t-phase of zirconia, but the peak height intensity of the main reflection of zirconia (Fig. 6) is twice stronger than that of acidic pH due to the crystal growth (Fig. 1c).

These results have been explained in terms of different stability constant of M–CA complex (M=metal) under different pH values [24,33]. Citric acid is a tri basic acid that can be dissociated in aqueous solution to $C_6H_7O_7^-$, $C_6H_6O_7^{2-}$ and $C_6H_5O_7^{3-}$, depending on the pH of solution. At low pH (pH ~2.0), $C_6H_7O_7^-$ is the prevailing species, which can interact with M^{n+} ($M=Zr^{4+}$) to form complex $M(C_6H_7O_7)^{n-1}$ [24]. At high pH (pH ~12), $C_6H_5O_7^{3-}$ becomes the predominant species, which can interact more strongly with M^{n+} to form stable complex $M(C_6H_7O_7)^{n-3}$. According to stability constant for the above reaction, it is noticeable that the stability constant is high at large pH values, implying that the concentration of free M^{n+} in the solution is decreased and the homogeneity of zirconia in the solution is increased.

Typical TEM image of zirconia nanocrystals with EG:CA mole ratio 5:1 calcined at 490 °C is shown in Fig. 7. Bright field TEM micrographs, as shown in Fig. 7a, shows very pack particles was obtained at acidic medium. With Dark field TEM image, it is better seen that the particle sizes of the synthesized powders are in the nano range and the particles even when agglomerated, consisted of fine crystallites with 10–20 nm diameters. Fig. 7c shows the as-prepared samples at alkali pH. This figure clearly indicates that sheet-like particles with the width of 20–35 nm were obtained. From TEM study (Fig. 7a) it can be observed that the particles, prepared at acidic pH, not been separated from each other (the boundary between grains were not clearly observed). In Fig. 7, it was seen that the particles were agglomerated. Why does this occur in polymeric sol–gel method? During calcination, the removal of gaseous products from combustion of organic mass of the gel, generates capillary forces on the particles, which brings more particles to in contact with each other. This results in more particle agglomeration, cluster formation and particle growth during the synthesis [32].

3.4. Probable formation mechanism

There are two chemical reactions involved in the Pechini process: (i) chelation between complex cations and an α-hydroxy carboxylic acid (citric acid or EDTA etc.), (ii) polyesterification of excess hydroxycarboxylic acid with ethylene glycol [24]. Citric acid (CA) and ethylene glycol (EG) form a couple most widely employed in the Pechini process. CA can form very stable chelating complexes with many metal ions, and these formed metal –CA complexes can be further stabilized in EG as it possesses two alcoholic hydroxyl functional groups (–OH) with strong complexation affinities to metal ions. Furthermore, two hydroxyl functional groups in one EG molecule can react with three carboxylic acid groups (–COOH) in one CA molecule to

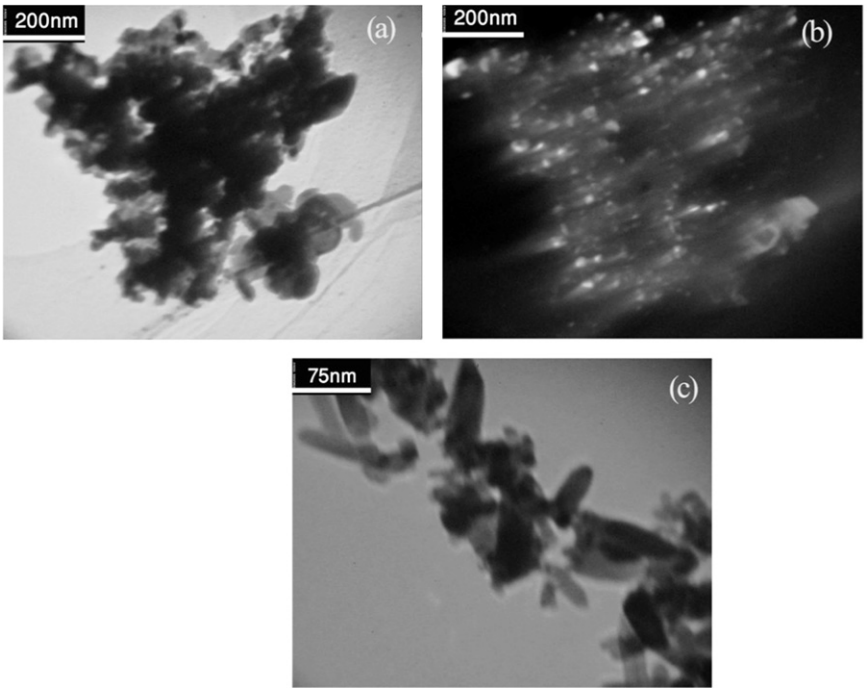

Fig. 7. TEM images of zirconia nanocrystals with EG:CA mole ratios 5:1 calcined at 490 °C at different pH (a and b) ~2 (c) 12.

form a polyester resin [19,25]. It is clear that ethylene glycol with alcohol and hydrocarbon chain in one molecule, provides versatile solvency characteristics with polar properties. However, the effect of EG and CA molecules on the particle size of products could be due to the steric hindrance [31,32]. The presence of excess EG:CA mole ratio (increasing EG:CA mole ratio from 1:1 to 5:1) plays the role of a space-filling template or capping agent and helps initial zirconia particles embedded, in the gel matrix, grow in 2D (sheet-like) particles.

It should also be noted that when the source of zirconium salt varied from $Zr(acac)_2$ to Zirconium acetate, at both alkali and acidic pH, the semi-spherical nanoparticles were obtained. This shows how the variation in precursor changes the morphologies of the products.

The main function of citric acid and EG is to provide a polymeric network to hinder cations mobility, which maintains local stoichiometry and minimizes the precipitation of unwanted phase. An increase in pH from 1 to 12 at 650 °C, caused carboxylic acid (–COOH) functional group of CA transform to carboxylate (COO^-). This group could react better with –OH group of EG and produce more polymeric resin with long chain, improving the uniformity of metal element in the solution and resin. Therefore, desegregated particles were observed in alkali medium (Fig. 5d).

3.5. Optical properties

The room temperature PL spectra, measured on zirconia nanocrystals with different morphologies such as nanoparticles (prepared with EG: CA 5:1) and nanosheets (prepared with EG: CA 20:1) are shown in Fig. 8(curves a–f). Upon excitation in the optical absorption region from 265 to 315 nm, an efficient blue luminescence, for the nanoparticles, centered at 460, 486.0, 497.5 nm were observed (Fig. 8a and b), while the nanosheets gives emissions in 430, 468 nm (Fig. 8a–c). The energies of the excitation lights (4.68–3.94 eV) are higher than the band gap energy of t-phase of zirconia (2.2–4.3 eV), suggesting that the PL is intrinsic [25,26,31]. Furthermore, the research showed that the apparent E_g value of t-zirconia were 4.3–4.5 eV for average particle size from 26 to 6 nm, respectively [25]. As can be seen in Fig. 8a–c, Fluorescence spectra were measured with several excitation wavelengths between 265 and 315 nm. While the fluorescence intensity changes to some extent with the excitation wavelength, the fluorescence band position and the band shape remained about the same for excitation wavelengths below 315 nm. This indicates that the fluorescence involves the same initial and final states even when the excitation wavelength varies from 265 to 315 nm. This result can be explained by fast relaxation from the final state reached by photo-excitation to those states from which the fluorescence originates.

The PL for the nanosheets prepared with EG:CA 20:1 (Fig. 8d–f) show a peak at 430 nm (2.88 eV photon energy with $\lambda_{exc}=265$ nm) while an emission centered at 468 nm (2.65 eV) with $\lambda_{exc}=290$ and 315 nm was observed. Fig. 8d–f, indicates that the fluorescence of nanosheets involves different initial and final states even when the excitation wavelength is varied between 265 and 315 nm.

4. Conclusions

The nanocrystalline tetragonal zirconia has been synthesized with reducing calcination temperature from 640 to 490 °C

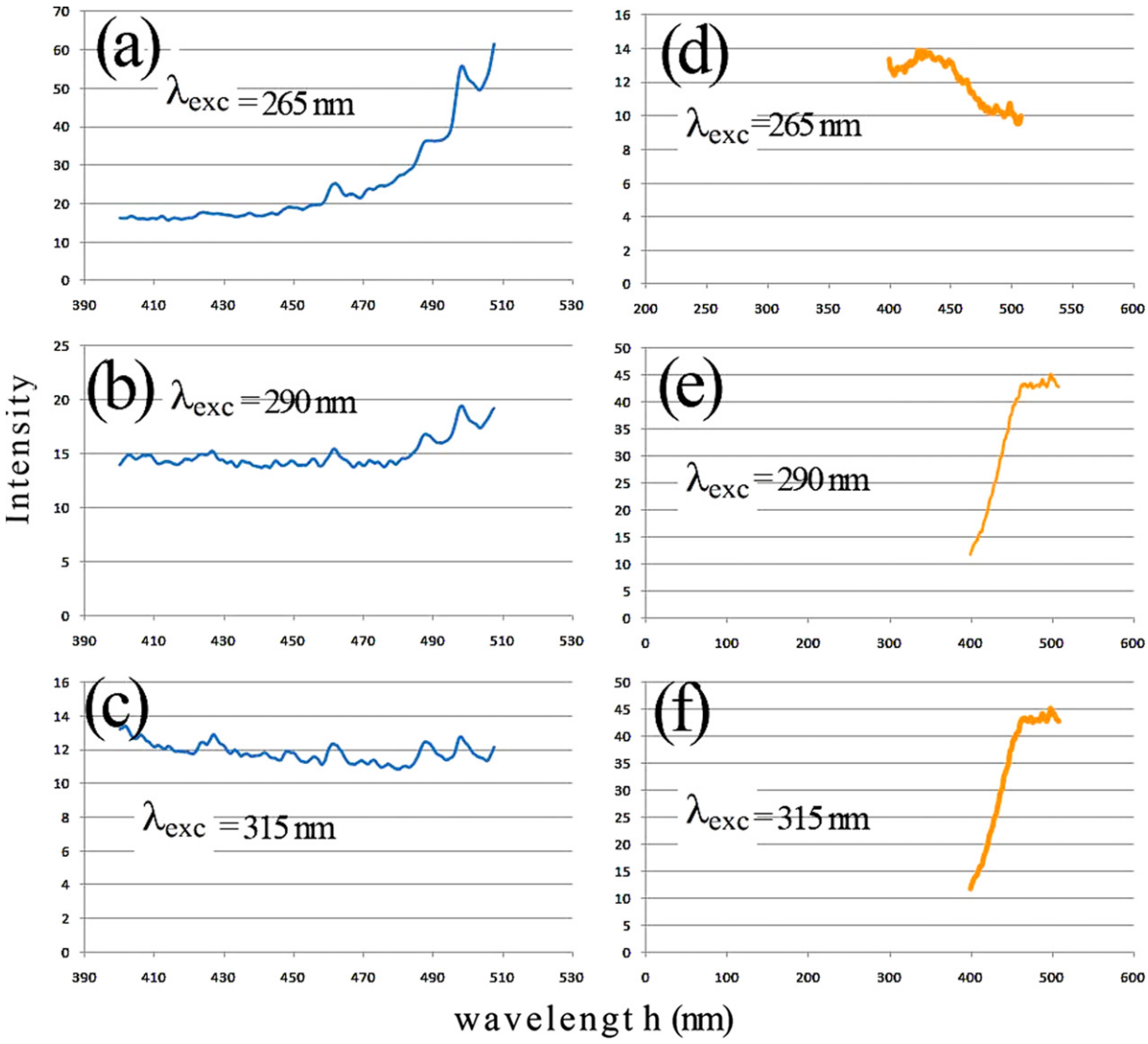

Fig. 8. PL spectra of ZrO_2 (a–c) nanopartciles prepared with EG:CA 5:1 and (d–f) nanosheets with EG:CA 20:1.

using by citric acid based sol–gel method. The SEM and TEM images show that the particle size of as-prepared samples with EG:CA 5:1, 490 °C/2 h are from 15 to 20 nm. The XRD patterns, obtained at the pH 1 and 12 precursors heated at 490 °C for 2 h, are similar to each other except that the relative intensities of product are greatly higher due to the crystal growth. The PL of zirconia nanoparticles has the same emission with varying excitation wavelength from 265 to 315 nm but zirconia nanosheets show different emissions.

References

[1] S.G. Botta, J.A. Navio, M.C. Hidalgo, G.M. Restrepo, M.I. Litter, Photocatalytic properties of ZrO_2 and Fe/ZrO_2 semiconductors prepared by a sol–gel technique, Journal of Photochemistry and Photobiology A: Chemistry 129 (1999) 89–99.

[2] E. Mustafa, M. Wilhelm, W Wruss, Phase stability and microstructural characteristics of 12 mol% (Mg, Ca)-PSZ prepared via polymeric route, Ceramics International 29 (2003) 189–194.

[3] M. Salavati-Niasari, M. Dadkhah, Pure cubic ZrO_2 nanoparticles by thermolysis of a new precursor, Polyhedron 28 (2009) 3005–3009.

[4] M. Salavati-Niasari, M. Dadkhah, Synthesis and characterization of pure cubic zirconium oxide nanocrystals by decomposition of bis-aqua, tris–acetylacetonato zirconium(IV) nitrate as new precursor complex, Inorganica Chimica Acta 362 (2009) 3969–3974.

[5] C. Viazzi, J.P. Bonino, F. Ansart, A. Barnabé, Structural study of metastable tetragonal YSZ powders produced via a sol–gel route, Journal of Alloys and Compounds 452 (2008) 377–383.

[6] D.S. Patil, K. Prabhakaran, Rajiv Dayal, C. Durga Prasad, N.M. Gokhale, A.B. Samui, S.C. Sharma, Eight mole percent yttria stabilized zirconia powders by organic precursor route, Ceramics International 34 (2008) 1195–1199.

[7] Y.W. Zhang, J.T. Jia, C.S. Liao, C.H. Yan, Synthesis of scandia-stabilized zirconia via thermo-decomposition of precursor complexes, Journal of Materials Chemistry 10 (2000) 2137 ± 2141.

[8] S.D. Kim, K.S. Hwang, Crystallinity, microstructure and mechanical strength of yttria-stabilized tetragonal zirconia ceramics for optical ferrule, Matials Science Applied 2 (2011) 1–5.

[9] F. Kazemi, F. Arianpour, S. Malek-Ahmadi, S. Sohrabi, H.R. Rezaie, A. Saberi, novel method for synthesis of metastable tetragonal zirconia nano powder at low temperatures, Materials

Research Bulletin (2011)http://dx.doi.org/10.1016/j.materresbull.2011.06.010.
[10] M. Shane, M.L. Mecartney, sol–gel synthesis of zirconia barrier coating, Journal of Materials Science 25 (1990) 1537–1544.
[11] N. Petrova, D. Todorovsky, Thermal decomposition of zirconium–yttrium citric complexes prepared in ethylene glycol and water media, Materials Research Bulletin 41 (2006) 576–589.
[12] H. Ch.Yao, X.W. Wang, H. Dong, R.R. Pei, J.S. Wang, Z.J. Li, Synthesis and characteristics of nanocrystalline YSZ powder by polyethylene glycol assisted coprecipitation combined with azeotropic-distillation process and its electrical conductivity, Ceramics International 37 (2011) 3153–3160.
[13] S. Farhikhteh, A. Maghsoudipour, B. Raissi, Synthesis of nanocrystalline YSZ (ZrO_2–$8Y_2O_3$) powder by polymerized complex method, Journal of Alloys and Compounds 491 (2010) 402–405.
[14] Ch.L. Robert, F. Ansart, C. Deloget, M. Gaudon, A. Rousset, Powder synthesis of nanocrystalline ZrO_2–$8\%Y_2O_3$ via a polymerization route, Materials Research Bulletin 36 (2001) 2083–2101.
[15] Ch.L. Robert, F. Ansart, S. Castillo, G. Richard, Synthesis of YSZ powders by the sol–gel method: surfactant effects on the morphology, Solid State Sciences 4 (2002) 1053–1059.
[16] Z. Ji, J.A. Haynes, U, M.K. Ferber, J.M. Rigsbee, Metastable tetragonal zirconia formation and transformation in reactively sputter deposited zirconia coatings, Surface and Coatings Technology 135 (2001) 109–117.
[17] S. Dosta, I.G. Cano, J.R. Miguel, J.M. Guilemany, Production and characterization of metastable ZrO_2–Al_2O_3 coatings obtained by APS quench, Journal of Thermal Spray Technology 360 (2008) 17.
[18] R Gomez, T. Lopez, Dehydroxylation and the crystalline phases in sol–gel zirconia, Journal of Sol–Gel Science and Technology 11 (1998) 309–319.
[19] X. Bokhimi, A. Morales, O. Novaro, M. Portilla, T. Lopez, F. Tzompantzi, R. Gomez, Tetragonal nanophase stabilization in nondoped sol–gel zirconia prepared with different hydrolysis catalysts, Journal of Solid State Chemistry 135 (1998) 8–35.
[20] R.C. Garvie, The occurrence of metastable tetragonal zirconia as a crystallite size effect, Journal of Physical Chemistry 69 (1965) 1238–1243.
[21] E. Crucean, B. Rand, Calcination of zirconia gels, British Ceramic Transactions 78 (1979) 58–64.
[22] D. Huang, K.R. Venkatachari, G.C. Stangle, Influence of yttria content on the preparation of nanocrystalline yttria-doped zirconia, Journal of Materials Research 10 (1995) 762–773.
[23] R. Dayal, N.M. Gokhale, S.C. Sharma, R. Krishnan, Investigation of the metastable tetragonal phase in yttria-doped zirconia powders prepared by a sol–gel technique, British Ceramic Transactions 91 (1992) 45–47.
[24] S. Sakka, H. Kozuka, Handbook of sol–gel science and technology processing, Characterization and Applications, second ed., Kluwer Academic Publishers, 2005 P 60–76.
[25] D. Ciuparu, A. Ensuque, G. Shafeev, F. Bozon-Verduraz, Synthesis and apparent bandgap of nanophase zirconia, Journal of Materials Science Letters 19 (2000) 931–933.
[26] G.H. Stout, L.H. Jensen, X-ray Structure Determination, second ed., John Wiley and Sons, 1989.
[27] M.M. Rashad, H.M. Baioumy, Effect of thermal treatment on the crystal structure and morphology of zirconia nanopowders produced by three different routes, Journal of Materials Processing Technology 195 (2008) 178–185.
[28] K.G. Kanade, J.O. Baeg, S.K. Apte, T.L. Prakash, B.B. Kale, Synthesis and characterization of nanocrystallined zirconia by hydrothermal method, Materials Research Bulletin 43 (2008) 723–729.
[29] R. Srinivasan, S.F. Simpson, J.M. Harris, B.H. Davis, Discrepancies in the crystal structures assigned to precipitated zirconia, Journal of Materials Science Letters 10 (1991) 352–354.
[30] K.K. Srivastava, R.N. Patil, C.B. Choudhary, K.V.G.K. Gokhale, E.C. Subba Rao, Revised phase diagram of the system ZrO_2–$YO_{1.5}$, Transactions and Journal of the British Ceramic Society 73 (1974) 85–91.
[31] F. Heshmatpour, R. Babadi-Aghakhanpour, Synthesis and characterization of superfine pure tetragonal nanocrystalline sulfated zirconia powder by a non-alkoxide sol–gel route, Advanced Powder Technology (2011)http://dx.doi.org/10.1016/j.apt.2010.12.012.
[32] K.A. Singh, L.C. Pathak, S.K. Roy, Effect of citric acid on the synthesis of nano-crystalline yttria stabilized zirconia powders by nitrate–citrate process, Ceramics International 33 (2007) 1463–1468.
[33] R. Shoja Razavi, M.R. Loghman-Estarki, M. Farhadi-Khouzani, M Barekat, H. Jamali, Large scale synthesis of zinc Oxide nano- and submicro-structure by Pechini's method: effect of ethylene glycol/citric acid mole ratio on structural and optical properties, Current NanoScience 7 (2011) 807–812.
[34] J. Liang, X. Jiang, G. Liu, Z. Deng, J. Zhuang, F. Li, Y. Li, Characterization and synthesis of pure ZrO_2 nanopowders via sonochemical method, Materials Research Bulletin 38 (2003) 161.
[35] A.G.H. Mekhemer, Characterization of phosphated zirconia by XRD Raman and IR spectroscopy, Colloids and Surfaces A: Physicochemical and Engineering Aspects 141 (1998) 227–235.